MODELING AND SIMULATION OF THIN SHEET FOLDING

SÖREN BARTELS, ANDREA BONITO, AND PETER HORNUNG

ABSTRACT. The article addresses the mathematical modeling of the folding of a thin elastic sheet along a prescribed curved arc. A rigorous model reduction from a general hyperelastic material description is carried out under appropriate scaling conditions on the energy and the geometric properties of the folding arc in dependence on the small sheet thickness. The resulting two-dimensional model is a piecewise nonlinear Kirchhoff plate bending model with a continuity condition at the folding arc. A discontinuous Galerkin method and an iterative scheme are devised for the accurate numerical approximation of large deformations.

1. INTRODUCTION

Because of their relevance in the development of new technologies bending theories for thin sheets have attracted considerable attention within applied mathematics in the past decades, with renewed activity following the seminal article [FJM02a]. In the present article the folding of thin elastic sheets along a prepared curved arc is considered which naturally leads to bending effects, cf. Figure 1. This setting has only been partially addressed mathematically, e.g., [DD82; BBH22], but has recently attracted considerable attention in applied sciences, cf., e.g. [Sch+15; CM19; PM19; PHL19; Cab+19; Liu+21] and references therein. Particular applications arise in the design of cardboxes and bistable switching devices that make use of corresponding flapping mechanisms. It is our aim to derive a mathematical description via a rigorous dimension reduction from three-dimensional hyperelasticity and to devise effective numerical methods that correctly predict large deformations in practically relevant settings.

To describe our approach we let $S \subset \mathbb{R}^2$ be a bounded Lipschitz domain that represents the midplane of an asymptotically thin sheet and let $\Sigma \subset S$ be a curve (with endpoints on ∂S) that models the crease, i.e., the arc along which the sheet is folded. The corresponding three-dimensional model involves a thickness parameter $h > 0$ and the thin domain $\Omega_h = S \times (-h/2, h/2)$. The material is weakened (or damaged) in a neighbourhood of width $r > 0$ around the arc Σ and we consider for given

Date: February 7, 2022.

2010 *Mathematics Subject Classification.* 74K20 74G65 65N30.

Key words and phrases. Nonlinear bending, folding, interface, model reduction, numerical method.

functions W and $f_{\varepsilon,r}$ the hyperelastic energy functional for a deformation $z : \Omega_h \to \mathbb{R}^3$

$$E^h(z) = \int_{\Omega_h} f_{\varepsilon,r}(x) W(\nabla z)\,\mathrm{d}x.$$

Here $f_{\varepsilon,r}(x) \in (0,1]$ is small with value $\varepsilon > 0$ close to the arc Σ and approximately 1 away from the arc, the function W is a typical free energy density. Hence, the factor $f_{\varepsilon,r}$ models a reduced elastic response of the material close to Σ. By appropriately relating the thickness h, the intactness fraction ε, and width r of the prepared region, we obtain for $(h, \varepsilon, r) \to 0$ a meaningful dimensionally reduced model which seeks a minimizing deformation $y : S \to \mathbb{R}^3$ for the functional

$$E_K(y) = \frac{1}{24} \int_{S\setminus\Sigma} Q(A)\,\mathrm{d}x',$$

where A is the second fundamental form related to the parametrization y which is weakly differentiable in S with second weak derivatives away from Σ, i.e., we consider

$$y \in W^{2,2}(S \setminus \Sigma; \mathbb{R}^3) \cap W^{1,\infty}(S; \mathbb{R}^3).$$

The quadratic form Q is obtained by a pointwise relaxation procedure of the Hessian of W. For isotropic materials it can explicitly be represented in terms of the Lamé coefficients, cf. [FJM02a]. Furthermore, the deformation y is required to satisfy the pointwise isometry condition

$$(\nabla y)^{\mathsf{T}}(\nabla y) = I,$$

which implies that no shearing and stretching effects occur. The minimization of E_K is supplemented by boundary conditions and possible body forces. Note that for our scaling of the parameters ε, r, and h, e.g., $\varepsilon = o(h)$ and $r = O(h)$, no energy contributions such as a penalization of the folding angle arise from the crease, i.e., the material can freely fold along the arc and y is in general only continuous on Σ. In our analysis, the damaged set is required to be wide enough to ensure that the strain of the folded sheet can easily remain of order one, and the damaged material should be soft enough to ensure that the energetic contribution of the fold becomes asymptotically negligible. On the other hand, if the damaged material is too soft, the sheet could fall apart; our compactness ensures the continuity of the asymptotic deformation across the fold.

In the absence of a crease Σ the model coincides with Kirchhoff's plate bending functional describing, e.g., the deformation of paper, which was rigorously derived in [FJM02a]. We slightly modify the arguments given there to take into account the fact that any asymptotic deformation which does not only bend but also folds has infinite Kirchhoff energy. This is because the Hessian corresponding to a folding deformation is not square integrable. Other variants of the setting from [FJM02a] have been addressed, in [Fri+03; FJM02b; HV18; Vel15; Sch07] and many others.

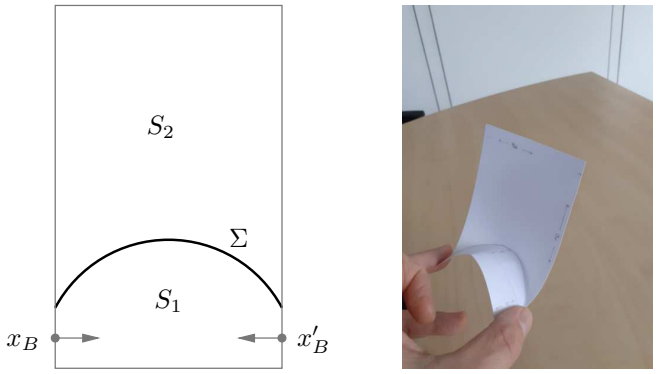

FIGURE 1. *Left:* Geometry of a prepared elastic sheet S with folding arc Σ that separates regions S_1 andf S_2; boundary conditions are imposed in the points x_B, x'_B. *Right:* When the boundary points x_B and x'_B are moved towards each other a flapping mechanism occurs.

A typical setting and an experiment are shown in Figure 1 and a coarse visual inspection indicates that the scaling relation $r \sim h$ together with a sufficiently strong compression of the material along the arc lead to the desired folding effect. Interesting phenomena take place at the folding arc. It was observed in [DD82] that a deformation on one side of the arc locally restricts possible deformations on the other side. In fact, only a finite number of scenarios is possible and either the gradients coincide along the arc resulting in a smooth deformation or a discontinuity occurs and the deformation is locally up to a sign uniquely determined. This important effect is a result of the isometry condition and the related physical property that thin elastic sheets are unshearable in the bending regime. Moreover, this effect arises in biology and inspires the development of new technologies and design in architecture [Sch+15].

Our numerical method to approximate minimizers is based on a discontinuous Galerkin method from [BNN21] which generalizes the approach based on a nonconforming method of [Bar13]. It allows us to define a discrete curve $\widetilde{\Sigma}$ as a union of element sides that approximates Σ and to account for possible discontinuities of deformation gradients along Σ by simply removing typical jump terms in the discrete formulation. The continiuity condition on the deformation y along the interface Σ is similar to a simple support boundary condition in linear bending theories. For such problems the plate paradox, cf. [BP90], states that convergence of approximations resulting from polyhedral approximations of curved domains or interfaces fails in general. We therefore consider piecewise quadratic approximations $\widetilde{\Sigma}$ of Σ. We note however that we do not observe significant differences to approximations obtained with piecewise linear arcs $\widetilde{\Sigma}$ in the nonlinear setting under consideration.

We assume for simplicity and without loss of generality that $Q(A) = |A|^2$ and use that the Frobenius norm of the second fundamental form equals the Frobenius norm of the Hessian in the case of an isometry y, i.e., $|A|^2 = |\nabla^2 y|^2$. Our numerical method then uses discontinuous deformations $\widetilde{Y} : S \to \mathbb{R}^3$ from an isoparametric finite element space $\widetilde{\mathbb{V}}^3 \subset L^2(S;\mathbb{R}^3)$ subordinated to a partitioning $\widetilde{\mathcal{T}}$ of S and a suitably defined discrete Hessian $\widetilde{H}(\widetilde{Y})$ in $S \setminus \widetilde{\Sigma}$ which define the discrete energy functional

$$\begin{aligned}\widetilde{E}_K(\widetilde{Y}) =& \frac{1}{24}\int_{S\setminus\Sigma} |\widetilde{H}(\widetilde{Y})|^2 \,\mathrm{d}x' \\ &+ \frac{\gamma_0}{2}\int_{\cup\widetilde{\mathcal{E}}^a} h_{\widetilde{\mathcal{E}}}^{-3} |[\![\widetilde{Y}]\!]|^2 \,\mathrm{d}s + \frac{\gamma_1}{2}\int_{\cup\widetilde{\mathcal{E}}^a\setminus\widetilde{\Sigma}} h_{\widetilde{\mathcal{E}}}^{-1} |[\![\widetilde{\nabla}\widetilde{Y}]\!]|^2 \,\mathrm{d}s.\end{aligned}$$

The last two terms are typical stabilization terms with the mesh-size function $h_{\widetilde{\mathcal{E}}}$ on the skeleton $\widetilde{\mathcal{E}}$ of the triangulation $\widetilde{\mathcal{T}}$ that guarantee coercivity and enforce continuity of $\widetilde{Y}$ and the elementwise gradient $\widetilde{\nabla} y$ across interelement sides or essential boundary conditions on certain boundary sides as the mesh-size tends to zero. The union of all such sides is the set of active sides which is denoted by $\widetilde{\mathcal{E}}^a$. Crucial here is that the penalized continuity of $\widetilde{\nabla}\widetilde{Y}$ is not imposed along the discrete folding arc $\widetilde{\Sigma}$ and that related consistency terms do not enter in the definition of the discrete Hessian $\widetilde{H}$. The important isometry condition is imposed up to a tolerance via a sum of integrals on elements, i.e., we require that

$$\widetilde{Y} \in \widetilde{\mathcal{A}} = \Big\{ \widetilde{Z} \in \widetilde{\mathbb{V}}^3 : \sum_{T\in\widetilde{\mathcal{T}}} \Big| \int_T (\widetilde{\nabla}\widetilde{Z})^{\mathsf{T}}(\widetilde{\nabla}\widetilde{Z}) - I \,\mathrm{d}x' \Big| \le \widetilde{\varrho} \Big\} \tag{1}$$

for a suitable tolerance $\widetilde{\varrho} > 0$. To obtain accurate approximations of large deformations choosing a small parameter is desirable. Its particular choice is dictated by available density results. If, e.g., the density of smooth folding isometries can be guaranteed similar to [Hor11] even a pointwise controlled violation criterion can be used; otherwise a condition $\widetilde{\varrho} \ge c' h_{\widetilde{\mathcal{T}}}$ has to be satisfied, cf. [BNN21]. Boundary conditions on a part of the boundary ∂S are included in the discrete problem via an appropriate definition of the jump terms. A justification of the discrete energy functionals via Γ convergence as in [Bar13; BBN17; BNN21] is in preparation.

The iterative solution of the constrained minimization problem follows the ideas of [Bar13; BBN17; BNN21] and is realized by a discrete gradient flow with a suitable linearization of the constraint. In particular, we consider the linear space $\widetilde{\mathcal{F}}[\widetilde{Z}]$ of variations for a given deformation $\widetilde{Z} \in \widetilde{\mathcal{A}}$ defined via

$$\widetilde{\mathcal{F}}[\widetilde{Z}] = \Big\{ \widetilde{W} \in \widetilde{\mathbb{V}}^3 : \int_T (\widetilde{\nabla}\widetilde{Z})^{\mathsf{T}}(\widetilde{\nabla}\widetilde{W}) + (\widetilde{\nabla}\widetilde{W})^{\mathsf{T}}(\widetilde{\nabla}\widetilde{Z}) \,\mathrm{d}x' = 0 \text{ for all } T \in \widetilde{\mathcal{T}} \Big\}.$$

We furthermore let $(\cdot,\cdot)_\star$ be an inner product and $\tau > 0$ a step size. Given an approximation $\widetilde{Y}^{k-1} \in \widetilde{\mathcal{A}}$ we look for a correction $d_t\widetilde{Y}^k \in \widetilde{\mathcal{F}}[\widetilde{Y}^{k-1}]$ such

that

$$\big(d_t\widetilde{Y}^k,\widetilde{V}\big)_\star+\widetilde{a}_K\big(\widetilde{Y}^{k-1}+\tau d_t\widetilde{Y}^k,\widetilde{V}\big)=0 \tag{2}$$

for all $\widetilde{V}\in\widetilde{\mathcal{F}}[\widetilde{Y}^{k-1}]$ and with the discrete bilinear form $\widetilde{a}_K$ associated with the discrete quadratic energy functional $\widetilde{E}_K$. The existence of a unique solution $d_t\widetilde{Y}^k$ is an immediate consequence of the Lax–Milgram lemma and we define the new approximation

$$\widetilde{Y}^k=\widetilde{Y}^{k-1}+\tau d_t\widetilde{Y}^k.$$

This implies the interpretation of the symbol d_t as a backward difference quotient. By choosing $\widetilde{V}=d_t\widetilde{Y}^k$ one directly obtains the energy decay property for $\ell=0,1,\dots,$

$$\widetilde{E}_K[\widetilde{Y}^\ell]+\tau\sum_{k=1}^{\ell}\|d_t\widetilde{Y}^k\|_\star^2\le\widetilde{E}_K[\widetilde{Y}^0]=\widetilde{E}_K^0$$

in particular, we see that $\|d_t\widetilde{Y}^k\|_\star\to0$ as $k\to\infty$, i.e., the iteration becomes stationary. Because of the orthogonality relation included in the space $\widetilde{\mathcal{F}}[\widetilde{Y}^{k-1}]$ we can bound the violation of the isometry constraint by repeatedly replacing $\widetilde{Y}^k=\widetilde{Y}^{k-1}+\tau d_t\widetilde{Y}^k$, i.e., for all $T\in\widetilde{\mathcal{T}}$ we have

$$\int_T[\widetilde{\nabla}\widetilde{Y}^\ell]^{\mathsf{T}}\widetilde{\nabla}\widetilde{Y}^\ell-I\,\mathrm{d}x'=\int_T[\widetilde{\nabla}\widetilde{Y}^0]^{\mathsf{T}}\widetilde{\nabla}\widetilde{Y}^0-I+\tau^2\sum_{k=1}^{\ell}[\widetilde{\nabla}d_t\widetilde{Y}^k]^{\mathsf{T}}\widetilde{\nabla}d_t\widetilde{Y}^k\,\mathrm{d}x'.$$

If the discrete gradient flow metric $(\cdot,\cdot)_\star$ controls the L^2 norm of the elementwise gradient, we obtain from the energy decay law the estimate

$$\sum_{T\in\widetilde{\mathcal{T}}}\Big|\int_T[\widetilde{\nabla}\widetilde{Y}^\ell]^{\mathsf{T}}\widetilde{\nabla}\widetilde{Y}^\ell-I\,\mathrm{d}x'\Big|\le\varepsilon^0+c_\star\widetilde{E}_K^0\tau,$$

where ε^0 is the initial isometry violation. In particular, we see that if τ and ε^0 are sufficiently small, an arbitrary accuracy can be achieved and we have $\widetilde{Y}^\ell\in\widetilde{\mathcal{A}}$ independently of the number of iterations $\ell\ge0$.

Using the numerical scheme we simulate various scenarios that are motivated by practical applications, e.g., how the shape of the folding arc affects the flapping mechanism, or address subtle analytical features of solutions, e.g., the occurrence of energy concentrations when the curve Σ has a kink. Besides that we illustrate the robustness of the numerical method with respect to the choice of stabilization parameters and discuss the construction of suitable deformations that serve as starting values in the discrete gradient flow. Our experiments show that large deformations in highly nontrivial settings can be accurately computed with moderate resolution.

The outline of the article is as follows. In Section 2 we describe the general setup and the dimensionally reduced model. Its rigorous derivation is given in Section 3. The discontinuous Galerkin finite element method is derived and stated in Section 4. Numerical experiments are reported in Section 5.

2. Preliminaries

2.1. **Hyperelasticity for plates.** For a bounded Lipschitz domain $S \subset \mathbb{R}^2$ we consider a plate of thickness $h > 0$ occupying the domain $\Omega_h = S \times I_h$ in the reference configuration. The elastic energy stored in the configuration determined by a deformation $z : \Omega_h \to \mathbb{R}^3$ is given by

$$\int_{\Omega_h} W(\nabla z)\,\mathrm{d}x.$$

Here W is a frame indifferent stored energy function and as in [FJM02a] we impose the following conditions:

- (H1) $W \in C^0(\mathbb{R}^{3\times 3})$ and $W \in C^2$ in a neighbourhood of $SO(3)$.
- (H2) W is frame indifferent, i.e., $W(F) = W(RF)$ for all $F \in \mathbb{R}^{3\times 3}$ and all $R \in SO(3)$. Moreover, $W(I) = 0$.
- (H3) There is a constant C such that $\operatorname{dist}^2_{SO(3)} \le CW$; here $\operatorname{dist}_{SO(3)} : \mathbb{R}^{3\times 3} \to [0,\infty)$ denotes the distance function from the set $SO(3)$.

To analyze the limiting behaviour as $h \to 0$ it is convenient to work on the fixed domain

$$\Omega = S \times I,$$

where $I = (-1/2, 1/2)$. We define a rescaled deformation $y^h : \Omega \to \mathbb{R}^3$ by setting $y^h(x', x_3) = z(x', hx_3)$. Then the (re-scaled) elastic energy is given by

$$\widetilde{E}^h(y^h) = \int_\Omega W(\nabla_h y^h)\,\mathrm{d}x,$$

where $\nabla_h y^h = (\nabla' y^h \mid \frac{1}{h}\partial_3 y^h)$ and $\nabla' = (\partial_1, \partial_2)$.

2.2. **Notation.** Throughout this article we use standard notation related to Sobolev spaces, e.g., $W^{s,p}(U;\mathbb{R}^\ell)$ denotes the set of s times weakly differentiable, $\mathbb{R}^\ell$-valued functions in L^p whose weak derivatives are p-integrable. L^p norms are often used without specifying a domain when there is no ambiguity, and we abbreviate the L^2 norm on S by $\|\cdot\|$. We occasionally omit target domains $\mathbb{R}^\ell$ when this is clear from the context. The open ball of radius $r > 0$ around a point $x \in \mathbb{R}^n$ is denoted by $B_r(x)$. For integral functionals ocurring below, it is often useful to specify their integration domains explicitly, e.g., we write

$$E(y;\tilde{S}) = \int_{\tilde{S}} F(y)\,\mathrm{d}x'.$$

For the canonical choice, e.g., $\tilde{S} = S$, this argument is usually omitted. For $S \subset \mathbb{R}^2$ we identify maps defined on S with their trivial extension to $S \times \mathbb{R}$.

2.3. **Folded plates.** Our aim is to modify the arguments from [FJM02a] in order to allow for folding effects along a prescribed curve, see Figure 1. In applications, the folding curve Σ is prescribed by weakening the material along it.

Throughout this article $S \subset \mathbb{R}^2$ is a bounded Lipschitz domain. From now

on $\Sigma \subset S$ is a Jordan arc with both endpoints on the same connected component of ∂S. More precisely, let $\sigma : [0,1] \to \mathbb{R}^2$ be continuous and injective, set $\Sigma = \sigma(0,1)$ and $\partial\Sigma = \{\sigma(0), \sigma(1)\}$ and assume that $\Sigma \subset S$ and that $\partial\Sigma$ is contained in one single connected component of ∂S. Then $S \setminus \Sigma$ consists of precisely two connected components S_1 and S_2. We assume, in addition, that Σ is such that both S_1 and S_2 are Lipschitz domains. This latter hypothesis entails a great deal of regularity on Σ. In particular, Σ is locally a Lipschitz graph. Therefore, the area of the sets

$$\Sigma_R = B_R(\Sigma) = \bigcup_{x\in\Sigma} B_R(x)$$

converges to zero as $R \downarrow 0$. As explained in the introduction, we let r_h, $\varepsilon_h > 0$ be parameters that define the width of the prepared region and the amount of the material intactness. We then define $f^h : S \to [0,\infty]$ by

$$f^h = \varepsilon_h \chi_{\Sigma_{r_h}} + 1 - \chi_{\Sigma_{r_h}}, \tag{3}$$

where χ_M denotes the characteristic function of a set M. With this we consider the (re-scaled) three-dimensional energy functional $E^h : W^{1,2}(\Omega;\mathbb{R}^3) \to [0,\infty]$

$$E^h(y) = \int_\Omega f^h(x') W\big(\nabla_h y^h(x)\big)\,\mathrm{d}x. \tag{4}$$

Passing to the thin film limit $h \to 0$ leads to a pointwise isometry constraint, but does not exclude and discontinuities of the gradients across the arc Σ: we are led to the set of asymptotically admissible deformations

$$\begin{aligned}\mathcal{A}(S,\Sigma) = \{u \in W^{1,2}(S;\mathbb{R}^3) \cap W^{2,2}(S\setminus\Sigma;\mathbb{R}^3) :\\ (\nabla u)^{\mathsf{T}}(\nabla u) = I \text{ a.e. on } S\}.\end{aligned}$$

The corresponding asymptotic energy functional $E_K : W^{1,2}(S;\mathbb{R}^3) \to [0,\infty]$ is defined as

$$E_K(y) = \begin{cases} \frac{1}{24}\int_{S\setminus\Sigma} Q(A)\,\mathrm{d}x' & \text{if } u \in \mathcal{A}(S,\Sigma),\\ +\infty & \text{otherwise.}\end{cases} \tag{5}$$

Here, A is the second fundamental form of the surface parametrized by y with unit normal $n = \partial_1 y \times \partial_2 y$, i.e.,

$$A = (\nabla n)^{\mathsf{T}}(\nabla y),$$

and Q is obtained by relaxing, over the third column and row, the quadratic form corresponding to the Hessian $D^2W(I)$ of W at the identity matrix, i.e.,

$$Q(A) = \min_{d\in\mathbb{R}^3} D^2W(I)[(A\,|\,d),(A\,|\,d)],$$

where for given $A \in \mathbb{R}^{2\times 2}$ the matrix $(A\,|\,d) \in \mathbb{R}^{3\times 3}$ is obtained by consistently appending a row and column defined by $d \in \mathbb{R}^3$. Note that by

hypotheses (H1)-(H3) we have the Taylor expansion

$$W(I+hF) = \frac{h^2}{2} D^2W(I)[F,F] + o(h^2)$$

for $F \in \mathbb{R}^{3\times 3}$ and $h > 0$.

Remarks 2.1. *(i) Observe that every $y \in \mathcal{A}(S,\Sigma)$ belongs to $W^{1,\infty}(S;\mathbb{R}^3)$, because $y \in W^{1,2}(S;\mathbb{R}^3)$ and its derivatives are bounded almost everywhere on S since $(\nabla y)^{\mathsf{T}}(\nabla y) = I$ almost everywhere. In particular, y is continuous on S.*
(ii) We recall that a Lipschitz function f is in $W^{2,2}(S\setminus\Sigma)$ precisely if there is an $F \in L^2(S;\mathbb{R}^{2\times 2})$ such that $\nabla^2 f = F$ in the sense of distributions on $S\setminus\Sigma$.

3. Gamma-Convergence

The purpose of this section is to prove the following result.

Theorem 3.1. *Let ε_h, $r_h \in (0,\infty)$ be null sequences satisfying*

$$\limsup_{h\to 0} \frac{h^2}{\varepsilon_h} < \infty \tag{6}$$

and

$$\limsup_{h\to 0} \frac{h}{r_h} < \infty \tag{7}$$

as well as

$$\limsup_{h\to 0} \frac{\varepsilon_h r_h}{h^2} = 0. \tag{8}$$

Define f^h as in (3), define E^h as in (4) and define E_K as in (5).
Then deformations with finite bending energy are compact and $\frac{1}{h^2}E^h$ Gamma-converges to E_K. More precisely:

(1) *Assume that $y^h \in W^{1,2}(\Omega,\mathbb{R}^3)$ are such that*

$$\limsup_{h\to 0} \frac{1}{h^2} E^h(y^h) < \infty.$$

Then there exists a subsequence (not relabelled) and $y \in \mathcal{A}(S,\Sigma)$ such that $y^h \rightharpoonup y$ weakly in $W^{1,2}(\Omega)$ and locally strongly in $W^{1,2}((S\setminus\Sigma)\times I)$.

(2) *Assume that $y^h \rightharpoonup y$ weakly in $W^{1,2}(\Omega)$. Then*

$$E_K(y) \le \liminf_{h\to 0} E^h(y^h).$$

(3) *Let $y \in W^{1,2}(\Omega)$. Then there exist $y^h \in W^{1,2}(\Omega)$ such that*

$$\lim_{h\to 0} \frac{1}{h^2} E^h(y^h) = E_K(y).$$

Remarks 3.2. *(i) The bound* (6) *ensures that the damaged material is not too soft. This is used in the proof of the compactness result, Part 1 of Theorem 3.1, as it rules out discontinuities of the asymptotic deformation across* Σ.
The bound (7) *requires the damaged part of the material to be wide enough with respect to the thickness of the sheet, while* (8) *asserts that the damaged portion of the material should be soft enough to ensure that the fold does not contribute to the asymptotic energy. Conditions* (7) *and* (8) *are used in Part 3 of Theorem 3.1, as they exclude excessive strain.*
(ii) Observe that (6) *through* (8) *are met, for instance, if* $\varepsilon_h \sim h^2$ *and* $r_h \sim h$.

Theorem 3.1 is a consequence of Proposition 3.3 and of Proposition 3.5 below. Both of them rely on arguments and results in [FJM02a].

3.1. **Compactness and lower bound.**

Proposition 3.3. *Let* ε_h, $r_h \downarrow 0$ *as* $h \downarrow 0$ *and assume that* (6) *is satisfied. If* $y^h \in W^{1,2}(S, \mathbb{R}^3)$ *satisfy*

$$\limsup_{h\to 0} \frac{1}{h^2} E^h(y^h) < \infty,$$

then there exists a map $y \in \mathcal{A}(S, \Sigma)$ *such that, after taking subsequences,* $y^h \rightharpoonup y$ *weakly in* $W^{1,2}(\Omega, \mathbb{R}^3)$ *and locally strongly in* $W^{1,2}((S \setminus \Sigma) \times I, \mathbb{R}^3)$ *as* $h \downarrow 0$. *Moreover,*

$$E_K(y; S_i) \le \liminf_{h\to 0} \frac{1}{h^2} E^h(y^h; S_i \times I) \text{ for } i = 1, 2.$$

Proof. We omit the index h in ε_h and r_h; the letter C denotes constants that do not depend on h. By the definition of f^h in (3) we have

$$\int_{\Omega\setminus(\Sigma_r\times I)} W(\nabla_h y^h)\,\mathrm{d}x \le Ch^2 \le C.$$

On the other hand, by (6),

$$\varepsilon \int_{\Sigma_r\times I} W(\nabla_h y^h)\,\mathrm{d}x = \int_{\Sigma_r\times I} f^h W(\nabla_h y^h)\,\mathrm{d}x \le Ch^2 \le C\varepsilon.$$

From hypothesis (H3) on W we deduce that

$$\int_\Omega \mathrm{dist}^2_{SO(3)}(\nabla_h y^h)\,\mathrm{d}x \le C \int_\Omega W(\nabla_h y^h)\,\mathrm{d}x \le C.$$

Hence $(\nabla_h y^h)$ is uniformly bounded in $L^2(\Omega)$ due to the hypotheses on W. This implies that there exists $y \in W^{1,2}(S)$ such that $y^h \rightharpoonup y$ weakly in $W^{1,2}(\Omega)$, after taking subsequences. Indeed, we first notice that (∇y^h) is uniformly bounded in $L^2(\Omega)$ and therefore, after taking a subsequence (not relabelled), we see that there is some $y \in W^{1,2}(\Omega)$ such that $y^h \rightharpoonup y$ weakly in $W^{1,2}(\Omega)$. Then we note that $\|\partial_3 y^h\|_{L^2(\Omega)} \le Ch \to 0$ implies that $\partial_3 y = 0$. Hence y does not depend on x_3 and therefore we can identify it with a map

(denoted by the same symbol) in $W^{1,2}(S)$.
Since $\int_{(S\setminus\Sigma_r)\times I)} W(\nabla_h y^h)\,\mathrm{d}x \le Ch^2$ and $r \to 0$, by monotonicity of the integral we conclude that for any (h-independent) $R > 0$ we have

$$\int_{(S\setminus\Sigma_R)\times I} W(\nabla_h y^h)\,\mathrm{d}x \le Ch^2$$

for all small enough h. The constant C does not depend on R.
Now fix a small $R > 0$ and define $S_i^R = S_i \setminus \Sigma_R$ for $i = 1, 2$; both are Lipschitz domains. We can apply [FJM02a, Theorems 4.1 and 6.1 (i)] on each S_i^R. Hence $y^h \to y$ strongly in $W^{1,2}(S_i^R \times I)$ and $y \in \mathcal{A}(S, \Sigma_R)$ with

$$\frac{1}{24}\int_{S_i^R} Q(A)\,\mathrm{d}x' \le \liminf_{h\to 0} h^{-2}\int_{S_i^R\times I} W(\nabla_h y^h)\,\mathrm{d}x \le C. \tag{9}$$

Here A is the second fundamental form of y on $S \setminus \Sigma_R = S_1^R \cup S_2^R$. Since y is an isometric immersion, by [FJM06, Proposition 6] we have

$$|\nabla^2 y| = |A| \text{ almost everywhere on } S \setminus \Sigma_R.$$

Hence (9) implies that

$$\|\nabla^2 y\|_{L^2(S_1^R)} + \|\nabla^2 y\|_{L^2(S_2^R)} \le C. \tag{10}$$

This is true for all R and the constant C does not depend on R. As noted earlier, the area of Σ_R converges to 0 as $R \to 0$. Hence $y \in W^{2,2}(S \setminus \Sigma)$ and

$$\int_{S_i} Q(A)\,\mathrm{d}x' = \limsup_{R\to 0}\int_{S_i^R} Q(A)\,\mathrm{d}x' < \infty.$$

Summarising, we have $y^h \to y$ locally strongly in $W^{1,2}((S \setminus \Sigma) \times I)$ and $y \in \mathcal{A}(S, \Sigma)$.
According to (9), for every small $R > 0$ we have

$$\begin{aligned} E_K(y; S_i^R) &\le \liminf_{h\to 0} h^{-2} E^h(y^h; S_i^R \times I) \\ &\le \liminf_{h\to 0} h^{-2} E^h(y^h; S_i \times I). \end{aligned}$$

The right-hand side does not depend on R. Taking the supremum over all small $R > 0$, we therefore see that

$$E_K(y; S_i) \le \liminf_{h\to 0} h^{-2} E^h(y^h; S_i \times I).$$

□

3.2. **Recovery sequence.** In the proof of Proposition 3.5 below we will use the following lemma.

Lemma 3.4. *Let $U \subset \mathbb{R}^2$ be a bounded Lipschitz domain. Then there exists a constant $\delta > 0$, depending only on the Lipschitz constant of U, such that the following is true: if $M \subset U$ satisfies $|M| < \delta(\operatorname{diam} U)^2$ and if we set*

$$R = \sqrt{\frac{2|M|}{\delta}},$$

then $B_R(x)$ intersects $U \setminus M$ for each $x \in U$.

Proof. This is standard; we include the proof for convenience. By Definition 1.3 in [Gia83, Chapter III] and the remark following it, there exists a constant $\delta > 0$, depending only on the Lipschitz constant of U, such that $|B_\rho(z) \cap U| \geq \delta \rho^2$ whenever $z \in U$ and $\rho < \operatorname{diam} U$.
If $B_R(x)$ did not intersect $U \setminus M$, then $B_R(x) \cap U \subset M$ and thus we would have

$$2|M| = \delta R^2 \leq |B_R(x) \cap U| \leq |M|,$$

a contradiction. □

The main result of this section is the following proposition.

Proposition 3.5. *Let ε_h, $r_h \in (0, \infty)$ be null sequences satisfying (7) and (8) and let $y \in \mathcal{A}(S, \Sigma)$. Then there exist $y^h \in W^{1,2}(\Omega, \mathbb{R}^3)$ such that $y^h \rightharpoonup y$ weakly in $W^{1,2}(\Omega, \mathbb{R}^3)$ and*

$$\lim_{h \downarrow 0} E^h(y^h) = E_K(y). \tag{11}$$

Proof. As before $S_{1,2}$ denote the connected components of $S \setminus \Sigma$. Denote the restriction of y to S_i by u_i and denote by n_i the normal to u_i. In this proof we will write ε instead of ε_h and r instead of r_h. The letter C denotes constants that do not depend on h as $h \downarrow 0$.
Let $U \subset \mathbb{R}^2$ be an open ball containing the closure of S. As each S_i is a Lipschitz domain, by [Ste70] we can extend each u_i and each n_i to maps

$$\begin{aligned} u_i &\in W^{2,2}(\mathbb{R}^2, \mathbb{R}^3) \cap W^{1,\infty}(\mathbb{R}^2, \mathbb{R}^3) \\ n_i &\in W^{1,2}(\mathbb{R}^2, \mathbb{R}^3) \cap L^{\infty}(\mathbb{R}^2, \mathbb{R}^3) \end{aligned} \tag{12}$$

supported in U. Notice that we use the same symbols to denote the extended maps as for the original ones. The norms of the extended maps can be bounded by those of the original ones, up to a factor that only depends on U, S and on Σ.
As in the proof of [FJM02a, Theorem 6.1 (ii)] we truncate the maps n_i and u_i and thus obtain sequences of maps n_i^h and u_i^h satisfying the bound

$$\|(\nabla')^2 u_i^h\|_{L^\infty(U)} + \|\nabla' n_i^h\|_{L^\infty(U)} \leq \frac{1}{h}, \tag{13}$$

while at the same time there is a set $M^h \subset S$ with

$$\limsup_{h \to 0} \frac{|M^h|}{h^2} = 0 \tag{14}$$

such that

$$u_i^h = u_i \text{ and } n_i^h = n_i \text{ on } S \setminus M^h. \tag{15}$$

Since $|M^h| \to 0$ by (14), Lemma 3.4 shows that there is a constant δ depending only on S and Σ, such that choosing

$$\rho_h = \sqrt{\frac{2|M^h|}{\delta}}$$

we have

$$B_{\rho_h}(x_0) \cap S \setminus M_h \neq \emptyset \text{ for all } x_0 \in S. \tag{16}$$

By (14) we have

$$\limsup_{h\to 0} \frac{\rho_h}{h} = 0. \tag{17}$$

We claim that, for $i = 1, 2$, the following L^∞ bounds are satisfied for a constant C depending only on y, S and Σ:

$$\frac{1}{\rho_h}|u_i^h - u_i| + |\nabla' u_i^h| + |n_i^h| \leq C \text{ almost everywhere on } S. \tag{18}$$

In fact, (12) implies that

$$|\nabla' u_i| + |n_i| \leq C \text{ almost everywhere on } \mathbb{R}^2. \tag{19}$$

Since $u_i^h = u_i$ (hence $\nabla' u_i^h = \nabla' u_i$) and $n_i^h = n_i$ almost everywhere on $S \setminus M^h$ by (15), we clearly have

$$|\nabla' u_i^h| + |n_i^h| \leq C \text{ almost everywhere on } S \setminus M^h. \tag{20}$$

On the other hand, (13) shows that the Lipschitz constants of $\nabla' u_i^h$ and of n_i^h on U are bounded by $1/h$. By (16), for all $x \in S$ there is a $y \in S \setminus M^h$ such that

$$|n_i^h(x)| \leq |n_i^h(y)| + |n_i^h(x) - n_i^h(y)| \leq C + \frac{1}{h}|x - y| \leq C + \frac{\rho_h}{h}.$$

Here we used (20) to estimate $|n_i^h(y)|$. In view of (17) this implies the bound on $|n_i^h|$ asserted in (18). The bound on $|\nabla' u_i^h|$ is proven similarly.
In particular, the Lipschitz constants of $u_i^h : S \to \mathbb{R}^3$ are uniformly bounded. Since u_i is Lipschitz as well, the maps $u_i^h - u_i$ are Lipschitz on S with uniformly bounded Lipschitz constants as $h \downarrow 0$. Since $u_i^h - u_i = 0$ on $S \setminus M^h$, we deduce from (16) that $|u_i^h - u_i| \leq C\rho_h$ on S. This concludes the proof of (18).
We will now define the recovery sequence. In order to do so, for each h let $\eta^h \in C^\infty(S, [0, 1])$ be a smooth cutoff function with $\eta^h = 1$ on $S_1 \setminus \Sigma_r$ and $\eta^h = 0$ on $S_2 \setminus \Sigma_r$; we choose it such that

$$\|\nabla' \eta^h\|_{L^\infty(\Sigma_r)} \leq \frac{C}{r}. \tag{21}$$

Set $\eta_1^h = \eta^h$ and $\eta_2^h = 1 - \eta^h$. Let $d \in W^{1,\infty}(S, \mathbb{R}^3)$ and define the recovery sequence

$$y^h(x', x_3) = \sum_{i=1}^{2} \Big(u_i^h(x') + h x_3 n_i^h(x') \Big) \eta_i^h(x') + h^2 \frac{x_3^2}{2} d(x'). \tag{22}$$

For later use we note that by this definition

$$\left| y^h - \sum_{i=1}^{2} u_i \eta_i^h \right| \leq h(|n_1^h| + |n_2^h|) + h^2 |d|.$$

Hence, in view of (18) we conclude that there is a constant C depending only on S, Σ and y such that

$$|y^h - y| \le Ch\,(1 + h|d|) \text{ on } (S \setminus \Sigma_r) \times I. \tag{23}$$

Now we compute

$$\begin{aligned}\nabla' y^h(x', x_3) = &\sum_{i=1}^{2} \Big(\nabla' u_i^h(x') + hx_3 \nabla' n_i^h(x')\Big)\, \eta_i^h(x') \\ &+ \sum_{i=1}^{2} \Big(u_i^h(x') + hx_3 n_i^h(x')\Big)\, \nabla' \eta_i^h(x') + h^2 \frac{x_3^2}{2} \nabla' d(x').\end{aligned}$$

Recalling that $\eta_1^h = \eta^h$ and $\eta_2^h = 1 - \eta^h$, we see that on $\Sigma_r \times I$

$$\begin{aligned}|\nabla' y^h| &\le \sum_{i=1}^{2} (|\nabla' u_i^h| + h|\nabla' n_i^h|) \\ &\quad + |u_1^h - u_2^h||\nabla' \eta^h| + h|n_1^h - n_2^h||\nabla' \eta^h| + h^2 |\nabla' d| \\ &\le C\big(1 + \frac{1}{r}|u_1^h - u_2^h| + \frac{h}{r}|n_1^h - n_2^h|\big).\end{aligned} \tag{24}$$

We have used the bound (21) as well as (18) and the estimate (13) for $\nabla' n_i^h$. Similarly, since

$$\partial_3 y(x', x_3) = h \sum_{i=1}^{2} n_i^h(x') \eta_i^h(x') + h^2 x_3 d(x'),$$

we can estimate

$$\frac{1}{h}|\partial_3 y^h| \le \sum_{i=1}^{2} |n_i^h \eta_i^h| + h|x_3 d| \le C(|n_1^h| + |n_2^h| + h) \le C, \tag{25}$$

in view of (18). Recalling (7), we deduce from (24) and (25) that

$$|\nabla_h y^h| \le C\big(1 + \frac{1}{r}|u_1^h - u_2^h|\big) \text{ on } \Sigma_r \times I. \tag{26}$$

Here we used (18) to estimate $|n_1^h - n_2^h|$ on the right-hand side of (24). We claim that

$$|u_1^h - u_2^h| \le Cr \text{ on } \Sigma_r. \tag{27}$$

To prove this, note that (18), (17) and (7) imply that

$$|u_i^h - u_i| \le C\rho_h \le Ch \le Cr \text{ on } S.$$

Hence it remains to show that

$$|u_1 - u_2| \le Cr \text{ on } \Sigma_r. \tag{28}$$

But $u_1 - u_2$ is Lipschitz on U in view of (12). Moreover it is zero on Σ because y is continuous. Hence (28) follows from the definition of Σ_r. This concludes the proof of (27).

By (27) and (26) we see that

$$\|\nabla_h y^h\|_{L^\infty(\Sigma_r\times I)} \le C.$$

Since W is locally bounded, this implies

$$\|W\big(\nabla_h y^h\big)\|_{L^\infty(\Sigma_r\times I)} \le C.$$

Therefore, since $|\Sigma_r| \le Cr$ due to the regularity of Σ,

$$\frac{1}{h^2}E^h(y^h,\Sigma_r\times I) = \frac{\varepsilon}{h^2}\int_{\Sigma_r\times I} W(\nabla_h y^h)\,\mathrm{d}x \le \frac{C\varepsilon r}{h^2}. \tag{29}$$

The right-hand side converges to zero due to (8).

On $S_i\setminus\Sigma_r$ the function η_i^h is identically equal to 1. Hence

$$\nabla_h y^h = (\nabla' u_i^h \mid n_i^h) + hx_3(\nabla' n_i^h \mid d) + \frac{h^2x_3^2}{2}(\nabla' d \mid 0) \text{ on } (S_i\setminus\Sigma_r)\times I. \tag{30}$$

The map $R = (\nabla' y \mid n)$ clearly takes values in $SO(3)$. Define

$$a_i^h = x_3R^{\mathsf T}(\nabla' n_i^h \mid d) + \frac{hx_3^2}{2}R^{\mathsf T}(\nabla' d \mid 0).$$

Then

$$|a_i^h| \le C(|\nabla' n_i^h| + |d| + h|\nabla' d|) \le C(1+|\nabla' n_i^h|). \tag{31}$$

Hence (13) ensures that, for small h,

$$h|a_i^h| \le C \text{ on } S. \tag{32}$$

On $S\setminus M^h$ we have $n_i^h = n_i$, hence $\nabla' n_i^h = \nabla' n_i$ almost everywhere on this set. Therefore, (31) shows that

$$|a_i^h| \le C(1+|\nabla' n_i|) \text{ on } S_i\setminus M^h. \tag{33}$$

By the frame indifference of W we have, almost everywhere on $(S_i\setminus\Sigma_r)\times I$,

$$W(\nabla_h y^h) = W\big(R^{\mathsf T}\nabla_h y^h\big) = W\big(R^{\mathsf T}(\nabla' u_i^h \,|\, n_i^h) + ha_i^h\big). \tag{34}$$

On $S_i\setminus M_h$ we have $(\nabla' u_i^h \,|\, n_i^h) = R$, so on $(S_i\setminus\Sigma_r\setminus M^h)\times I$

$$\begin{aligned}\frac{1}{h^2}W(\nabla_h y^h) &= \frac{1}{h^2}W(I+ha_i^h)\\ &\le \frac{C}{h^2}\operatorname{dist}^2_{SO(3)}(I+ha_i^h) \le C|a_i^h|^2.\end{aligned}$$

We have used (32) and the fact that the hypotheses on W imply that $W \le C\operatorname{dist}^2_{SO(3)}$ on bounded subsets of $\mathbb{R}^{3\times3}$. Now (33) implies the bound

$$\frac{1}{h^2}\chi_{S_i\setminus M_h}W(I+ha_i^h) \le C(1+|\nabla' n_i|^2). \tag{35}$$

The right-hand side is in $L^1(S_i)$ and does not depend on h. On the other hand, by Taylor expansion and since $|\Sigma_r|\to 0$ and $|M^h|\to 0$

$$\frac{1}{h^2}\chi_{(S_i\setminus\Sigma_r\setminus M_h)\times I}W(I+ha_i^h) \to \frac{1}{2}Q_3\big(x_3R^{\mathsf T}(\nabla' n_i \,|\, d)\big)$$

pointwise almost everywhere on $S_i \times I$. Combining this with (35) we can apply dominated convergence to conclude

$$\frac{1}{h^2} E^h(y^h, (S_i \setminus \Sigma_r \setminus M_h) \times I) \to \frac{1}{24} \int_{S_i} Q_3(R^{\mathsf{T}}(\nabla' n_i \,|\, d))\, \mathrm{d}x'. \tag{36}$$

We now claim that

$$\limsup_{h \to 0} \|W\big(\nabla_h y^h\big)\|_{L^\infty((S \setminus \Sigma_r) \times I)} < \infty. \tag{37}$$

In fact, since W is locally bounded, (37) will follow once we show that

$$\|\nabla_h y^h\|_{L^\infty((S \setminus \Sigma_r) \times I)} \leq C. \tag{38}$$

But by (30), on $(S_i \setminus \Sigma_r) \times I$ we have

$$|\nabla_h y^h| \leq C \left(1 + |\nabla' u_i^h| + |n_i^h| + h|\nabla' n_i^h|\right).$$

The last term on the right-hand side is uniformly bounded due to (13), whereas the other two are uniformly bounded due to (18). This concludes the proof of (37).
Using (37) we see that

$$\frac{1}{h^2} E^h(y^h, (M_h \setminus \Sigma_r) \times I) = \frac{1}{h^2} \int_{(M^h \setminus \Sigma_r) \times I} W(\nabla_h y^h) \leq \frac{C}{h^2} |M_h|. \tag{39}$$

By (14) the right-hand side converges to zero as $h \to 0$. Summarizing, by combining (29), (36) and (39) we see that

$$\frac{1}{h^2} E^h(y^h) \to \frac{1}{24} \int_S Q_3(R^{\mathsf{T}}(\nabla' n \,|\, d))\, \mathrm{d}x',$$

where n is the normal to y. Relaxing over $d \in L^2$ as in [FJM02a], the convergence (11) follows.
More precisely, there exist $d_j \in W^{1,\infty}(S, \mathbb{R}^3)$ converging strongly in L^2 and a sequence $h_j \to 0$ such that, defining y^{h_j} as in (22) with $d = d_j$, the convergence (11) is true for $h = h_j$. Proposition 3.3 implies that, after taking a subsequence, (y^{h_j}) converges weakly in $W^{1,2}(\Omega)$ to some $\widetilde{y} \in \mathcal{A}(S, \Sigma)$. Since the d_j remain uniformly bounded in L^2, estimate (23) ensures that $\widetilde{y} = y$. □

4. Discretization

We devise in this section a discretization of the folding problem based on the use of an isoparametric discontinuous Galerkin finite element method. Corresponding functions and related discrete quantities are marked by a tilde sign.

4.1. **Finite element spaces.** We follow [BNN21] and let $\widetilde{\mathcal{T}}$ be a partition of the Lipschitz domain S into closed, shape regular elements $T \in \widetilde{\mathcal{T}}$ which are images of mappings $F_T : \widehat{T} \to T$, where $\widehat{T}$ is a reference triangle or square. The space $\widetilde{\mathbb{V}}$ of discontinuous piecewise transformed polynomials of fixed polynomial degree $k \geq 2$ is defined as

$$\widetilde{\mathbb{V}} = \{\widetilde{V} \in L^2(S) : \widetilde{V} \circ F_T \in P_k \cup Q_k \text{ for all } T \in \widetilde{\mathcal{T}}\},$$

where P_k and Q_k denote polynomials of total and partial degree k on the respective reference element. We let $\widetilde{\mathcal{E}}^{int}$ be the set of interior edges.

The elementwise application of a differential operator is indicated by a tilde, e.g., for $\widetilde{V} \in \widetilde{\mathbb{V}}$ we define

$$\widetilde{\nabla}\widetilde{V}|_T = \nabla(\widetilde{V}|_T)$$

for all $T \in \widetilde{\mathcal{T}}$. We use standard notation to denote jumps and averages of elementwise smooth functions, e.g.,

$$[\![\widetilde{V}]\!]_e = \widetilde{V}^+ - \widetilde{V}^-, \quad \{\widetilde{V}\}_e = (\widetilde{V}^+ + \widetilde{V}^-)/2,$$

for an inner side $e = T^+ \cap T^-$ with a fixed unit normal μ_e pointing from T^+ into T^- that determines the sign of $[\![\widetilde{V}]\!]$.

To match the targeted experiments, the boundary conditions imposed in all the numerical simulations provided below are pointwise Dirichlet boundary conditions, i.e. we enforce $y(x_i^D) = g_i$, where x_i is a vertex of the subdivision on the boundary of S and g_i are given boundary deformations, $i = 1, ..., n_D$. Whence, the jump and average operators do not need to be defined on boundary edges as in the free boundary case [Bon+21] unlike the clamped boundary case [BNN21].

4.2. **Curve approximation.** We assume throughout that the folding curve Σ is Lipschitz continuous and piecewise C^2 with possible kinks only occurring at vertices of the subdivision. Moreover, we assume that either a parametric description $\Sigma = \{\gamma(u), u \in [0,1]\}$ or, provided that Σ is C^2, the distance d_Σ to the curve is available. We also assume that the triangulation defines a piecewise smooth curve

$$\widetilde{\Sigma} = \cup_{j=1}^J e_j$$

with inner sides $e_j \in \widetilde{\mathcal{E}}^{int}$, $j = 1, \ldots, J$, such that the endpoints of the segments e_j belong to Σ. This implies that there exists a bijection $\widetilde{M} : \widetilde{\Sigma} \to \Sigma$ such that the distance between the two curves is small in the sense that

$$\|\widetilde{M} - \mathrm{id}\,\|_{W^{1,\infty}(\widetilde{\Sigma})} \to 0 \tag{40}$$

as $h \to 0$.

4.3. **Discrete Hessian.** To obtain good consistency properties of the approximate Hessian $\widetilde{H}(\widetilde{V})$ of a function $\widetilde{V} \in \widetilde{\mathbb{V}}$ we first note that the distributional Hessian $\mathrm{D}^2\widetilde{V}$ is for $\phi \in C_c^\infty(S \setminus \widetilde{\Sigma}; \mathbb{R}^{2\times 2})$ on the open set $S \setminus \widetilde{\Sigma}$ given by

$$\begin{aligned}\langle \mathrm{D}^2\widetilde{V}, \phi\rangle &= \int_{S\setminus\widetilde{\Sigma}} \widetilde{V} \operatorname{div}\operatorname{Div}\phi \,\mathrm{d}x' \\ &= \int_{S\setminus\widetilde{\Sigma}} \widetilde{D}^2\widetilde{V} : \phi \,\mathrm{d}x' + \sum_{e\in\widetilde{\mathcal{E}}^{int}\setminus\widetilde{\Sigma}} \int_e [\![\widetilde{V}]\!]\big(\operatorname{Div}\phi\cdot\mu_e\big) - [\![\widetilde{\nabla}\widetilde{V}]\!]\cdot\big(\phi\mu_e\big)\,\mathrm{d}s,\end{aligned}$$

where Div denotes the application of the standard divergence operator to the columns of a matrix-valued function. We aim at preserving this identity for elementwise polynomial functions $\widetilde{\phi}$ and represent the contributions on the interior edges $\widetilde{\mathcal{E}}^{int}$ by functions defined in the edge patches $\omega_e = T^- \cup T^+$. We follow ideas from [Pry14; BNN21] and define the operators

$$s_e : L^2(e;\mathbb{R}) \to \widetilde{\mathbb{V}}^{2\times 2}|_{\omega_e}, \quad r_e : L^2(e;\mathbb{R}^2) \to \widetilde{\mathbb{V}}^{2\times 2}|_{\omega_e},$$

for inner edges $e \in \widetilde{\mathcal{E}}^{int}$ via

$$\begin{aligned}\int_{\omega_e} s_e(\widehat{v}) : \widetilde{\phi}\,\mathrm{d}x' &= \int_e \widehat{v}\big\{\operatorname{Div}_h\widetilde{\phi}\cdot\mu_e\big\}\,\mathrm{d}s,\\ \int_{\omega_e} r_e(\widehat{w}) : \widetilde{\phi}\,\mathrm{d}x' &= \int_e \widehat{w}\cdot\big\{\widetilde{\phi}\mu_e\big\}\,\mathrm{d}s,\end{aligned}$$

for all $\widetilde{\phi} \in \widetilde{\mathbb{V}}^{2\times 2}|_{\omega_e}$; the functions $s_e(\widehat{v})$ and $r_e(\widehat{w})$ are trivially extended to S. We then define $\widetilde{H}(\widetilde{V}) \in \widetilde{\mathbb{V}}^{2\times 2}$ as

$$\widetilde{H}(\widetilde{V}) = \widetilde{D}^2\widetilde{V} + S_{\mathcal{E}}(\widetilde{V}) - R_{\mathcal{E}}(\widetilde{\nabla}\widetilde{V}),$$

where

$$S_{\mathcal{E}}(\widetilde{V}) = \sum_{e\in\widetilde{\mathcal{E}}^{int}} s_e([\![\widetilde{V}]\!]), \quad R_{\mathcal{E}}(\widetilde{\nabla}\widetilde{V}) = \sum_{e\in\widetilde{\mathcal{E}}^{int}\setminus\widetilde{\Sigma}} r_e([\![\widetilde{\nabla}\widetilde{V}]\!]).$$

Note that the contributions $S_{\mathcal{E}}$ associated with the continuity of y contains the edges on $\widetilde{\Sigma}$ while these are omitted in $R_{\mathcal{E}}$ respecting possible discontinuities in deformation gradients.

For every $\widetilde{\phi} \in \widetilde{\mathbb{V}}^{2\times 2} \cap C_c^1(S \setminus \widetilde{\Sigma}; \mathbb{R}^{2\times 2})$ we have the consistency property

$$\langle \mathrm{D}^2\widetilde{V}, \widetilde{\phi}\rangle = \int_U \widetilde{H}(\widetilde{V}) : \widetilde{\phi}\,\mathrm{d}x'.$$

In general the intersection $\widetilde{\mathbb{V}}^{2\times 2} \cap C_c^1(S \setminus \widetilde{\Sigma}; \mathbb{R}^{2\times 2})$ only contains constant functions. When the interface Σ is exactly captured by the subdivisions, i.e. $\widetilde{\Sigma} = \Sigma$, then the reconstructed Hessian restricted to any subdomain separated by Σ weakly converge to the continuous Hessian in L^2 [Bon+21].

We define a discrete seminorms approximating a seminorm of $W^{2,2}(S\setminus\Sigma)\cap W^{1,2}(S)$ for $\widetilde{V}\in\widetilde{\mathbb{V}}$ via

$$\|\widetilde{V}\|_{\widetilde{H}^2}^2=\|D_h^2\widetilde{V}\|^2+\int_{\widetilde{\mathcal{E}}^{int}}h_{\widetilde{\mathcal{E}}}^{-3}|[\![\widetilde{V}]\!]|^2\,\mathrm{d}s+\int_{\widetilde{\mathcal{E}}^{int}\setminus\widetilde{\Sigma}}h_{\widetilde{\mathcal{E}}}^{-1}|[\![\widetilde{\nabla}\widetilde{V}]\!]|\,\mathrm{d}s.$$

Note that the identity $\|\widetilde{V}\|_{\widetilde{H}^2}=0$ only implies that $\widetilde{V}$ is continuous and piecewise affine. By using standard inequalities we find that the discrete Hessian defines a bounded operator in the sense that

$$\|\widetilde{H}(\widetilde{V})\|\le c\|\widetilde{V}\|_{\widetilde{H}^2}$$

for all $\widetilde{V}\in\widetilde{\mathbb{V}}$ with a constant $c>0$ that is independent of the cardinality of $\widetilde{\mathcal{T}}$.

4.4. **Discrete energy functional.** Our discrete energy functional is defined on a discrete admissible set that enforces the isometry condition up to a tolerance $\widetilde{\varrho}>0$, i.e., we set

$$\widetilde{\mathcal{A}}=\Big\{\widetilde{Z}\in\widetilde{\mathbb{V}}^3:\sum_{T\in\widetilde{\mathcal{T}}}\Big|\int_T(\widetilde{\nabla}\widetilde{Z})^{\mathsf{T}}(\widetilde{\nabla}\widetilde{Z})-I\,\mathrm{d}x'\Big|\le\widetilde{\varrho}\Big\}.$$

The discrete functional $\widetilde{E}_K$ is then obtained by replacing the Hessian by its discrete approximation which is applied componentwise and introducing stabilizing and penalty terms, i.e., for $\gamma_0,\gamma_1,\gamma_2>0$ and $\widetilde{Y}\in\widetilde{\mathcal{A}}$ we set

$$\begin{aligned}\widetilde{E}_K(\widetilde{Y})=&\frac{1}{24}\int_{S\setminus\widetilde{\Sigma}}|\widetilde{H}(\widetilde{Y})|^2\,\mathrm{d}x'\\&+\frac{\gamma_0}{2}\int_{\widetilde{\mathcal{E}}^{int}}h_{\widetilde{\mathcal{E}}}^{-3}|[\![\widetilde{Y}]\!]|^2\,\mathrm{d}s+\frac{\gamma_1}{2}\int_{\widetilde{\mathcal{E}}^{int}\setminus\widetilde{\Sigma}}h_{\widetilde{\mathcal{E}}}^{-1}|[\![\widetilde{\nabla}\widetilde{Y}]\!]|^2\,\mathrm{d}s\\&+\frac{\gamma_2}{2}\sum_{i=1}^{n_D}h_i^{-2}[(\widetilde{Y}-g_i)(x_i^D)]^2.\end{aligned}$$

Assuming an isotropic material we have up to a constant factor $Q(A)=|A|^2$; we note that the approach applies to more general quadratic forms. Note that unlike in previous works, pointwise Dirichlet conditions are considered and enforced via penalization; h_i denotes a local meshsize around the vertex x_i^D.

The energy functional $\widetilde{E}_K$ is uniformly coercive in $\widetilde{H}^2$, i.e., there exists a constant c such that for any choice of parameters $\gamma_0,\gamma_1,\gamma_2>0$ we have for all $\widetilde{Y}\in\widetilde{\mathbb{V}}^3$

$$\|\widetilde{Y}\|_{\widetilde{H}^2}\le c_1\widetilde{E}_K(\widetilde{Y}),\qquad\widetilde{Y}\in\widetilde{\mathbb{V}}^3.$$

Furthermore, the gradients of deformations in the discrete admissible set $\widetilde{\mathcal{A}}$ are uniformly bounded:

$$\|\widetilde{\nabla}\widetilde{Y}\|\le\sqrt{2}\,(\widetilde{\varrho}+|S|)\,,\qquad\forall\widetilde{Y}\in\widetilde{\mathcal{A}}.$$

We refer to [Bon+21] for proofs of the above two inequalities. Note that these two estimates do not provide a uniform L^2 control. As a consequence, depending on the boundary conditions, the deformations may be defined up to certain invariances. If the gradient flow metric controls the L^2 norm, then the discrete gradient provides unique iterates.

A rigorous justification of the discrete energy functional $\widetilde{E}_K$ can be obtained by establishing its Gamma convergence to E_K as the maximal mesh-size h tends to zero. To prove the stability bound or liminf inequality one uses the coervity estimate and follows [BNN21; Bon+21] to show by using regularizations obtained with quasi-interpolation operators that for a sequence $(\widetilde{Y})_{h>0}$ with $\widetilde{E}_K(\widetilde{Y}) \leq c$ there exists a subsequence and a limit $y \in W^{2,2}(S \setminus \Sigma; \mathbb{R}^3) \cap W^{1,\infty}(S; \mathbb{R}^3)$ such that in $L^2(S)$ we have for $h \to 0$

$$\widetilde{Y} \to y, \quad \widetilde{\nabla}\widetilde{Y} \to \nabla y, \quad \widetilde{H}(\widetilde{Y}) \rightharpoonup D^2 y,$$

provided that elements $T \in \widetilde{\mathcal{T}}$ satisfy a geometric condition away from the discrete interface $\widetilde{\Sigma}$. The consistency or limsup inequality requires the construction of suitable interpolants $\widetilde{\mathcal{I}}y \in \widetilde{\mathcal{A}}$ of a given folding isometry $y \in W^{2,2}(S \setminus \Sigma; \mathbb{R}^3) \cap W^{1,\infty}(S; \mathbb{R}^3)$ such that

$$\widetilde{E}_K(\widetilde{\mathcal{I}}y) \to E_K(y)$$

as $h \to 0$. Crucial here is to show that on curved elements $T \in \widetilde{\mathcal{T}}$ along the discrete folding arc $\widetilde{\Sigma}$ the difference of the local energy contributions

$$\Big| \int_T |\widetilde{D}^2 \widetilde{\mathcal{I}}y|^2 \,\mathrm{d}x' - \int_{\widehat{T}} |D^2 y|^2 \,\mathrm{d}x' \Big|$$

with the corrected element $\widehat{T}$ hat has a side on the exact interface can be sufficiently controlled. Corresponding details are in preparation.

5. Numerical experiments

We report in this section on numerical results obtained with the proposed numerical method and the iterative scheme.

5.1. **Algorithmic aspects.** Except for the presence of folding curves and correspondingly removed edge contributions in the discontinuous Galerkin method the overall strategy follows closely the algorithm devised in [Bon+20] and later analyzed in [Bon+21]. The efficiency of the discrete gradient flow (2) for finding stationary configurations depends strongly on the availability of a good starting value, in particular on its discrete energy $\widetilde{E}_K^0$ and the isometry violation $\widetilde{\varrho}$, see (1). We note that the boundary conditions are included in a weak, penalized form and, in practice, constitute a major contribution of the initial energy when the initial deformation is not suitably constructed. To obtain an initial deformation with simultaneously moderate discrete bending energy $\widetilde{E}_K^0$ and small isometry violation $\widetilde{\varrho}$, we use the preprocessing procedure described in [Bon+20]. It combines the solution of a linear bi-harmonic problem to obtain an approximate discrete extension

$\widehat{Y}^0 \in \widetilde{\mathbb{V}}^3$ of the boundary data with a subsequent gradient descent applied to the isometry violation error with an iteration until this quantity is below a given tolerance, i.e., until the iterate $\widehat{Y}^L \in \widetilde{\mathbb{V}}^3$ satisfies

$$\frac{1}{2}\int_S |(\widetilde{\nabla}\widehat{Y}^L)^{\mathsf{T}}(\widetilde{\nabla}\widehat{Y}^L) - I|^2 \,\mathrm{d}x \le \varepsilon_{pp}.$$

We then define $\widetilde{Y}^0 = \widehat{Y}^L$ as the starting value for the gradient scheme (2). The gradient flow metric $(\cdot,\cdot)_*$ is obtained as a combination of the bilinear form defined by the discrete energy functional and the L^2 norm. With this choice we avoid nonuniqueness effects for certain boundary conditions. As a stopping criterion for this iteration we impose the condition that the discrete bending energy is nearly stationary, i.e.,

$$\left|d_t\widetilde{E}_K(\widetilde{Y}^M)\right| = \frac{\left|\widetilde{E}_K(\widetilde{Y}^M) - \widetilde{E}_K(\widetilde{Y}^{M-1})\right|}{\tau} \le \varepsilon_{stop},$$

for a given tolerance $\varepsilon_{stop} > 0$. The deformation $\widetilde{Y}^M \in \widetilde{\mathbb{V}}^3$ serves as our approximation of stationary, low energy configuration for $\widetilde{E}_K^0$ in the admissible set $\widetilde{\mathcal{A}}$. Unless specified otherwise, piecewise polynomials of degree 2 are used for the approximation of the deformation, the lifting operators in the construction of the discrete Hessian, and in approximating the folding curve by edges of elements. Our subdivisions are generated with the package `Gmesh` [GR09], the implementations make use of the `deal.ii` library [BHK07], and the visualization are obtained using `Paraview` [Squ+07].

5.2. **Bistable flapping device.** Our first set of experiment considers the setting sketched in Figure 1. The precise parameters defining the domain S and the arc Σ are as follows.

Example 5.1 (Parabolic and circular arcs)**.** *For $S = (0, 9.6) \times (0, 15)$ we consider compressive boundary conditions of rate $s \in (0, 1)$ imposed at the corners*

$$x_D = (0, 0), \quad x_D' = (9.6, 0.0).$$

Two choices of a folding arc $\Sigma \subset \overline{S}$ are addressed:
(a) Let Σ be the quadratic curve connecting two boundary points $x_{\Sigma,j} \in \partial S$, $j = 1, 2$, and passing through the apex $x_{\Sigma,A}$ given by

$$x_{\Sigma,1} = (0, 2), \quad x_{\Sigma,2} = (9.6, 2), \quad x_{\Sigma,A} = (4.8, 6).$$

(b) Let Σ be the circular arc with end-points $x_{\Sigma,j} \in \partial S$, $j = 1, 2$, and circular midpoint $x_{\Sigma,M} \notin \Sigma$ given by

$$x_{\Sigma,1} = (0, 2), \quad x_{\Sigma,2} = (9.6, 2), \quad x_{\Sigma,M} = (4.8, -2),$$

i.e., with radius $r^2 = (4.8)^2 + 4^2$.

A typical triangulation with 556 elements together with an exact resolution of the parabolic arc defined in Example 5.1 (a) is shown in Figure 2. Note that the arc is matched exactly by edges of elements. The simulations

are performed for a pseudo-time step $\tau = 0.01$ and tolerances $\varepsilon_{stop} = 0.01$, $\varepsilon_{pp} = 1.0$. The numerical approximations $\widetilde{Y}^M \in \widetilde{\mathbb{V}}^3$ obtained with the numerical scheme for different compression rates imposed in the boundary points x_D and x'_D are shown in Figure 3. We observe a good qualitative agreement with the real experiment shown in the left part of Figure 1 and a continuous dependence of the deformation on the compression rate. Only $0, 5, 10, 15$ iterations of the gradient descent method for compression rates $s = 0\%, 10\%, 20\%$, and 30% were required to meet the prescribed stopping criterion.

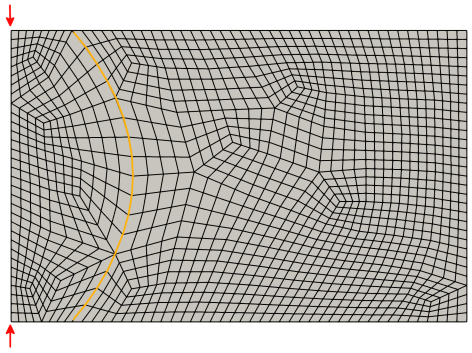

FIGURE 2. Triangulation, folding arc approximation, and compressive point boundary conditions to generate a bistable flapping mechanism described by Example 5.1 with a quadratic arc Σ that is resolved exactly.

When the folding arc is circular instead of parabolic then our discrete curves Σ_h do not resolve the goemetry exactly. For the setting described in Example 5.1 (b) and a triangulation consisting again of 556 elements that provide a piecewise quadratic approximation Σ_h of Σ we obtained for the parameter choices $\tau = 0.01$, $\varepsilon_{stop} = 0.1$, and $\varepsilon_{pp} = 1$ the nearly stationary configurations shown in Figure 4. The discrete deformations are similar to those obtained for the parabolic arc except that the deformed right side of the initial rectangular plate is now curved.

The effect of approximating the folding arc by a polygonal, piecewise straight curve is illustrated in Figure 5. The plots display the deformations obtained for the circular arc approximated accurately with piecewise quadratic edges of elements to a coarse approximation using three straight segments. The Frobenius norm of the Hessian, i.e., an approximation of the mean curvature of the deformed plates is visualized via a gray scale coloring. We see that energy concentrations occur at the kinks of the piecewise linear arc while a more uniform distribution arises for the circular arc with moderate peaks at the boundary where the compressive boundary condition is imposed and where the arc ends. Apart from that the overall deformation

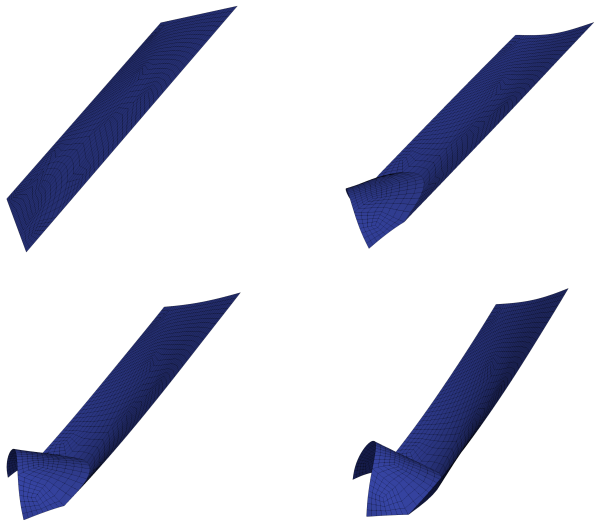

FIGURE 3. Nearly stationary configurations $\widetilde{Y}^M \in \widetilde{\mathbb{V}}^3$ in Example 5.1 with quadratic folding arc for compression rates $s = 0\%, 10\%$, 20%, and 30% (left to right, top to bottom).

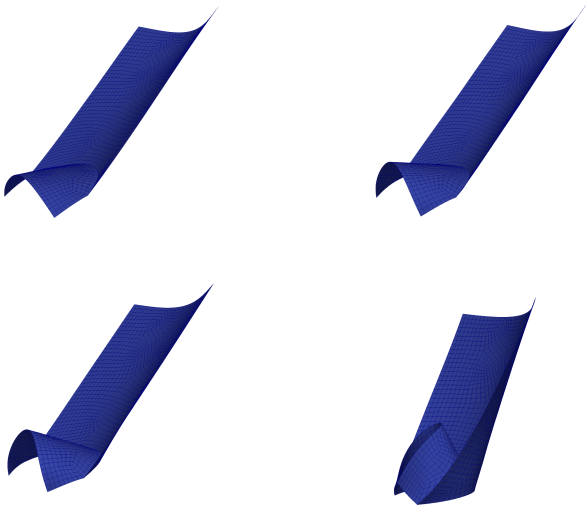

FIGURE 4. Nearly stationary configurations $\widetilde{Y}^M \in \widetilde{\mathbb{V}}^3$ in Example 5.1 with circular folding arc for compression rates $s = 10\%$, 20%, 30%, and 100%.

does not differ significantly and the main difference is a less curved plate away from the arc for the coarse, piecewise linear approximation.

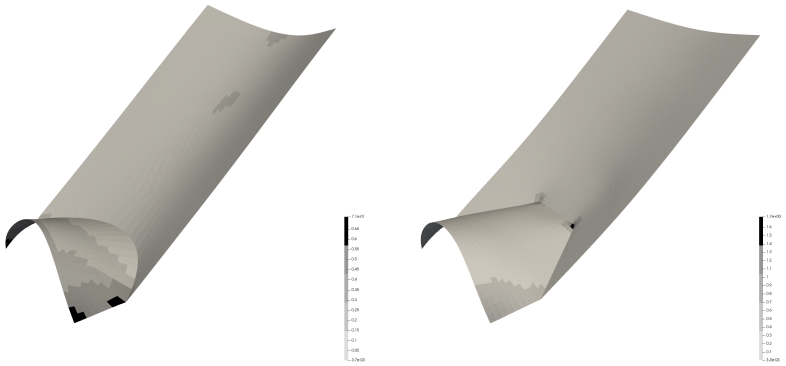

FIGURE 5. Different approximations of a circular folding arc using a piecewise quadratic segments (left) and piecewise linear segments (right) lead to different energy contributions but similar deformations. The colors represent the average curvature over each element of the subdivision. The ranges are from 0 (white) to 0.71 (black) for the quadratic folding line and from 0 (white) to 1.7 (black) for the piecewise linear folding line.

5.3. **Paper cutting and bending.** Our second experiment simulates a typical origami folding construction with curved arcs which is also known as kirigami folding which includes cutting and bending a piece of paper. In our example a square domain with a square hole is prepared using four arcs that connect midpoints of the outer boundary with the corners of the inner boundary, cf. Figure 6. The precise settings are as follows.

Example 5.2 (Flower configuration)**.** *Let* $S = (0,16) \times (0,16) \setminus S'$*, where* S' *is the square with defined by the vertices* $x_1 = (6,7)$*,* $x_2 = (7,10)$*,* $x_3 = (10,9)$*, and* $x_4 = (9,6)$*. We use four cubic Bezier curves that connect the midpoints* $x_{M,1} = (8,0)$*,* $x_{M,2} = (16,8)$*,* $x_{M,3} = (8,16)$*, and* $x_{M,4} = (0,8)$ *of the outer sides of* S *with the points* x_3, x_2, x_1, x_4*, respsectively, using suitable control points, e.g., for the first arc* Σ^1 *we use*

$$\widehat{x}_{1,1} = (10 + 3\cos(\alpha) - \sin(\alpha), 9 - \cos(\alpha) - 3\sin(\alpha)),$$
$$\widehat{x}_{1,2} = (8 + 3.162\cos(\alpha), 3.162\sin(\alpha)),$$

with $\alpha = \pi/6$*. Control points for the arcs* Σ^ℓ*,* $\ell = 2,3,4$*, are obtained via rotational point symmetry, cf. Figure 6. Compressive boundary conditions with* $s = 60\%$ *compression rate are imposed at the opposite boundary points* $x_{M,1}$ *and* $x_{M,3}$*.*

The setting and a photo of the result of a real experiment corresponding to Example 5.2 are shown in Figure 6.

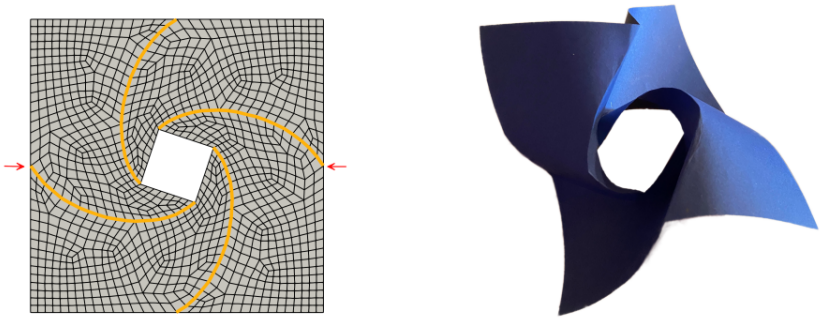

FIGURE 6. Geometric setting of Example 5.2 (left) and result of a real experiment with $s = 60\%$ compression rate (right).

Numerical solutions for Example 5.2 for different compression rates are shown in Figure 7. We used a triangulation with 1904 elements, a pseudo-time step $\tau = 0.025$, termination tolerances $\varepsilon_{stop} = 0.3$, $\varepsilon_{pp} = 0.5$. The discrete, nearly isometric deformations obtained with our numerical scheme reveal a remarkable similarity to configurations obtained in real experiments.

Acknowledgments. The authors SB and PH acknowledge support by the DFG via the priority programme SPP 2256 *Variational Methods for Predicting Complex Phenomena in Engineering Structures and Materials* (BA 2268/7-1, HO 4697/2-1). The author AB is partially supported by NSF grant DMS-2110811.

REFERENCES

[Bar13] S. Bartels. "Approximation of large bending isometries with discrete Kirchhoff triangles". In: *SIAM J. Numer. Anal.* 51.1 (2013), pp. 516–525. DOI: 10.1137/110855405.

[BBH22] S. Bartels, A. Bonito, and P. Hornung. *Folded isometric immersions*. In preparation. 2022.

[BBN17] S. Bartels, A. Bonito, and R. H. Nochetto. "Bilayer plates: model reduction, Γ-convergent finite element approximation, and discrete gradient flow". In: *Comm. Pure Appl. Math.* 70.3 (2017), pp. 547–589. DOI: 10.1002/cpa.21626.

[BHK07] W. Bangerth, R. Hartmann, and G. Kanschat. "deal.II – a General Purpose Object Oriented Finite Element Library". In: *ACM Trans. Math. Softw.* 33.4 (2007), pp. 24/1–24/27.

[BNN21] A. Bonito, R. H. Nochetto, and D. Ntogkas. "DG approach to large bending plate deformations with isometry constraint". In: *Math. Models Methods Appl. Sci.* 31.1 (2021), pp. 133–175. DOI: 10.1142/S0218202521500044.

[Bon+20] A. Bonito, D. Guignard, R. H. Nochetto, and S. Yang. *LDG approximation of large deformations of prestrained plates*. 2020. arXiv: 2011.01086 [math.NA].

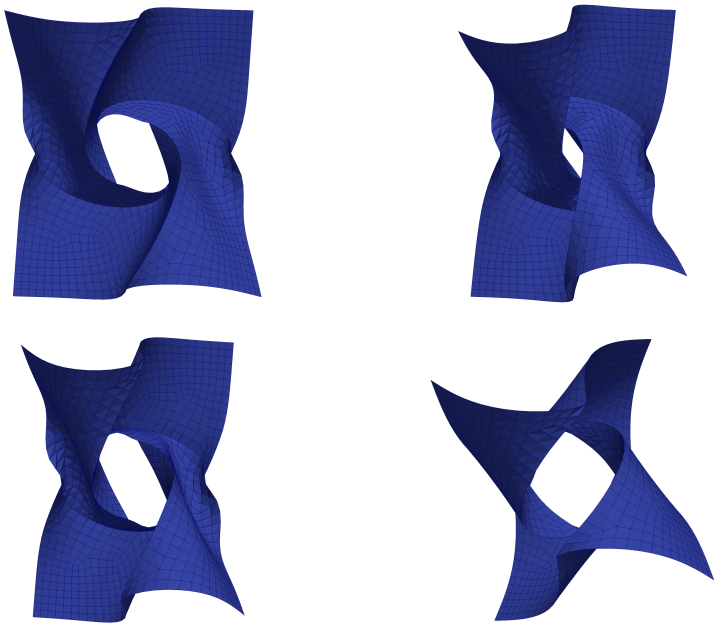

FIGURE 7. Discrete, nearly stationary deformations for 37.5%, 55%, 57.5%, and 60% compression rates (left to right, top to bottom).

[Bon+21] A. Bonito, D. Guignard, R. H. Nochetto, and S. Yang. *Numerical analysis of the LDG approximation of large deformations of prestrained plates*. 2021. arXiv: 2106.13877 [math.NA].

[BP90] I. Babuška and J. Pitkäranta. "The plate paradox for hard and soft simple support". In: *SIAM J. Math. Anal.* 21.3 (1990), pp. 551–576. DOI: 10.1137/0521030.

[Cab+19] A. Caboussat, R. Glowinski, D. Gourzoulidis, and M. Picasso. "Numerical approximation of orthogonal maps". In: *SIAM J. Sci. Comput.* 41.6 (2019), B1341–B1367. DOI: 10.1137/19M1243683.

[CM19] S. Chen and L. Mahadevan. "Rigidity percolation and geometric information in floppy origami". In: *Proceedings of the National Academy of Sciences* 116.17 (2019), pp. 8119–8124. DOI: 10.1073/pnas.1820505116. eprint: https://www.pnas.org/content/116/17/8119.full.pdf.

[DD82] J. P. Duncan and J. L. Duncan. "Folded developables". In: *Proc. Roy. Soc. London Ser. A* 383.1784 (1982), pp. 191–205.

[FJM02a] G. Friesecke, R. D. James, and S. Müller. "A theorem on geometric rigidity and the derivation of nonlinear plate theory from three-dimensional elasticity". In: *Comm. Pure Appl. Math.* 55.11 (2002), pp. 1461–1506. DOI: 10.1002/cpa.10048.

[FJM02b] G. Friesecke, R. D. James, and S. Müller. "The Föppl-von Kármán plate theory as a low energy Γ-limit of nonlinear elasticity". In: *C. R. Math. Acad. Sci. Paris* 335.2 (2002), pp. 201–206. DOI: 10.1016/S1631-073X(02)02388-9.

[FJM06] G. Friesecke, R. D. James, and S. Müller. "A hierarchy of plate models derived from nonlinear elasticity by gamma-convergence". In: *Arch. Ration. Mech. Anal.* 180.2 (2006), pp. 183–236. DOI: 10.1007/s00205-005-0400-7.

[Fri+03] G. Friesecke, R. D. James, M. G. Mora, and S. Müller. "Derivation of nonlinear bending theory for shells from three-dimensional nonlinear elasticity by Gamma-convergence". In: *C. R. Math. Acad. Sci. Paris* 336.8 (2003), pp. 697–702. DOI: 10.1016/S1631-073X(03)00028-1.

[Gia83] M. Giaquinta. *Multiple integrals in the calculus of variations and nonlinear elliptic systems*. Vol. 105. Annals of Mathematics Studies. Princeton University Press, Princeton, NJ, 1983, pp. vii+297.

[GR09] C. Geuzaine and J.-F. Remacle. "Gmsh: A 3-D finite element mesh generator with built-in pre-and post-processing facilities". In: *International journal for numerical methods in engineering* 79.11 (2009), pp. 1309–1331.

[Hor11] P. Hornung. "Approximation of flat $W^{2,2}$ isometric immersions by smooth ones". In: *Arch. Ration. Mech. Anal.* 199.3 (2011), pp. 1015–1067. DOI: 10.1007/s00205-010-0374-y.

[HV18] P. Hornung and I. Velčić. "Regularity of intrinsically convex $W^{2,2}$ surfaces and a derivation of a homogenized bending theory of convex shells". In: *J. Math. Pures Appl. (9)* 115 (2018), pp. 1–23. DOI: 10.1016/j.matpur.2018.04.008.

[Liu+21] H. Liu, P. Plucinsky, F. Feng, and R. D. James. "Origami and materials science". In: *Philosophical Transactions of the Royal Society A: Mathematical, Physical and Engineering Sciences* 379.2201 (2021), p. 20200113. DOI: 10.1098/rsta.2020.0113.

[PHL19] E. A. Peraza Hernandez, D. J. Hartl, and D. C. Lagoudas. *Active Origami*. Springer International Publishing, 2019, pp. xxi+464. DOI: 10.1007/978-3-319-91866-2.

[PM19] L. H. D. P. T. Choi and L. Mahadevan. "Programming shape using kirigami tessellations". In: *Nature Materials* 18.9 (2019), pp. 999–1004.

[Pry14] T. Pryer. "Discontinuous Galerkin methods for the p-biharmonic equation from a discrete variational perspective". In: *Electron. Trans. Numer. Anal.* 41 (2014), pp. 328–349.

[Sch+15] S. Schleicher, J. Lienhard, S. Poppinga, T. Speck, and J. Knippers. "A Methodology for Transferring Principles of Plant Movements to Elastic Systems in Architecture". In: *Comput. Aided Des.* 60.C (Mar. 2015), pp. 105–117. DOI: 10.1016/j.cad.2014.01.005.

[Sch07] B. Schmidt. "Plate theory for stressed heterogeneous multilayers of finite bending energy". In: *J. Math. Pures Appl. (9)* 88.1 (2007), pp. 107–122. DOI: 10.1016/j.matpur.2007.04.011.

[Squ+07] A. H. Squillacote, J. Ahrens, C. Law, B. Geveci, K. Moreland, and B. King. *The paraview guide*. Vol. 366. Kitware Clifton Park, NY, 2007.

[Ste70] E. M. Stein. *Singular integrals and differentiability properties of functions*. Princeton Mathematical Series, No. 30. Princeton University Press, Princeton, N.J., 1970, pp. xiv+290.

[Vel15] I. Velčić. "On the derivation of homogenized bending plate model". In: *Calc. Var. Partial Differential Equations* 53.3-4 (2015), pp. 561–586. DOI: 10.1007/s00526-014-0758-1.

Abteilung für Angewandte Mathematik, Albert-Ludwigs-Universität Freiburg, Hermann-Herder-Str. 10, 79104 Freiburg i. Br., Germany
Email address: bartels@mathematik.uni-freiburg.de

Texas A& M University, College Station, TX 77843, USA
Email address: bonito@tamu.edu

Fakultät Mathematik, Technische Universität Dresden, Zellescher Weg 12–14, 01069 Dresden, Germany
Email address: peter.hornung@tu-dresden.de